

Soft MAX phases with boron substitution: A computational prediction

Poulami Chakraborty,¹ Aurab Chakrabarty,¹ Amlan Dutta,² and Tanusri Saha-Dasgupta^{3,1}

¹*Department of Condensed Matter Physics and Materials Science, S. N. Bose National Centre for Basic Sciences, JD Block, Sector III, Salt Lake, Kolkata 700106, India*

²*Department of Metallurgical and Materials Engineering, Indian Institute of Technology Kharagpur, Kharagpur 721302, India*

³*Center for Mathematical, Computational and Data Science, Indian Association for the Cultivation of Science, Kolkata 700032, India*



(Received 19 June 2018; published 31 October 2018)

With a goal to improve upon the mechanical properties of the MAX phase, materials of high technological interest, we explore boron substitution in these compounds. Employing first-principles density functional theory (DFT) calculations, combined with continuum modeling to access the core structure of dislocations, we investigate the effect of boron-substitution on plastic deformation properties of a typical MAX phase compound, V_2AlC . Our $T = 0$ K results show that, due to the differential nature of chemical bonding between V and B compared to that between V and C, both V-Al and V-B basal slip planes get activated in boron-substituted compounds, compared to only V-Al basal slip in the parent compound. This, in turn, makes the boron compounds significantly more ductile compared to their carbide counterpart V_2AlC . The computation of temperature-dependent free energies of stable and unstable stacking faults further reveals the important and interesting role of thermal fluctuations in the deformation behavior of the boride compounds at elevated temperature. This suggests a change in the microscopic mechanism of plastic deformation upon varying temperature condition in the proposed boron compounds. Our study should motivate future exploration of boron-based MAX compounds.

DOI: [10.1103/PhysRevMaterials.2.103605](https://doi.org/10.1103/PhysRevMaterials.2.103605)

I. INTRODUCTION

The layered ternary carbides and/or nitrides with the general formula $M_{n+1}AX_n$, $n = 1, 2, 3$ were first discovered in powdered form way back in the 1960s [1–4]. They received renewed interest in the 1990s primarily due to the studies by Barsoum and coworkers [5,6], which highlighted the attractive properties of these compounds. These compounds, popularly known as “MAX” phases, consist of slabs of early transition metal carbide/nitride ($M_{n+1}X_n$) separated by single atomic layer of A element, where A is generally Al or Si or Ge. The laminate structure of the MAX phase compounds is responsible for making them machinable, damage tolerant, corrosion resistive on top of being good thermal and electrical conductors [7]. Given the unprecedented combination of desired properties, the research on MAX phase has become important both from the fundamental as well as from the application point of view. The number of research publications on MAX phase has shown almost an exponential increase in the past decade, reflecting the enthusiasm and rapid progress in the field.

Among many different exciting properties, the mechanical properties of MAX phases are of special interest. While the MAX phases share many physical and chemical properties with their corresponding MX phases, the mechanical properties of the two families are very different. The major obstacle for the use of MX phase is that they are quite stiff. The primary motivation of deriving MAX phase from MX phase, is to make the material soft and machinable to increase their application possibility. Due to the layered structure of the MAX compounds, the plastic deformation is primarily governed by slips in the basal plane [0001] [6], with dislocations arranged

in walls or pileups. This results in kink band formation [8], a suggested mechanism of plastic deformation of MAX phases at room temperature [9]. The understanding and tailoring of mechanical properties of this technologically important class of compounds are thus intimately connected to the knowledge of the dislocation behavior. The difference in the bonding characteristic between different atomic layers of the MAX phase leads to drastic inhomogeneity in the basal slips for different layers. In the MAX phase geometry, the transition metal M and group IV/V element X are bound with a strong covalent bond. A basal slip between the M and X layer is therefore energetically expensive and practically improbable. On the other hand, the M-A bond is of a softer nature and a slip between the M and A layers is more common [6,10–12].

The challenges for the immediate future of this potential field is to explore new phases in facilitating their applications. In the M_2AX (211) compounds, which is the largest family of MAX phase and is in the focus of this work, the three constituents are stacked as M-X-M-A. The M and X atoms forms a close-packed M_6X octahedra (see left panel in Fig. 1) which binds the M and X layers firmly. Therefore, one of the keys to tailor the mechanical properties would be to replace the X element with elements that are of similar ionic size but with significantly different chemical characteristics. One such possibility can be the use of the group III element, which shares the same row as IV or V (e.g., B instead of C or N). Boron forms weaker covalent bond compared to that of C or N, and it has been found previously that substituting B for C can dramatically alter the properties [13,14]. Properties of carbides and nitrides that constitute known 211 MAX phases are explored to a reasonable extent [6,15]. However, a boride has never been tested as a MAX phase. This would

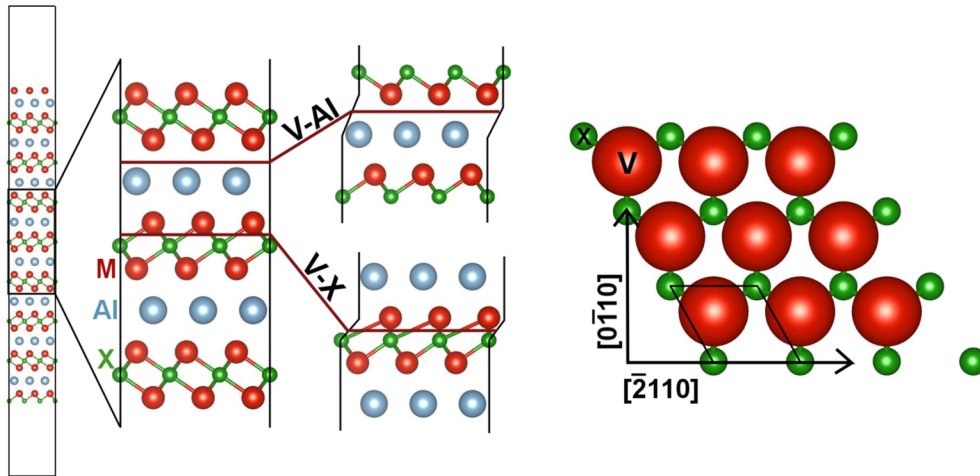


FIG. 1. Left panel: Crystal structure of V_2AlX ($X = C/B$) MAX phase with the two slip planes highlighted in the zoomed picture. Right panel: The top view of the structure in the $[0\bar{1}10]$ - $[\bar{2}110]$ plane. Marked in the picture is the hexagonal unit cell.

open up possible creation of new MAX phases with varied physical properties. In the present study, using a combination of *ab initio* and model calculations, we explore the effect of B substitution for C on mechanical properties of 211 MAX phase for the representative case of V_2AlC . The MAX phase compound V_2AlC was synthesized in bulk form back in 2004 [16], by isostatic pressing of V, Al, and C, and its elastic properties have been studied to a good extent [17–20]. The prediction on boron-substitution in V_2AlC thus can be readily checked.

Our computational study predicts that complete or partial replacement of C by B, in the carbide based MAX compound can cause a significant change in the mechanical properties of these compounds. In particular, boron substitution can make the material far more ductile by making basal slip planes involving both M-A and M-X planes energetically accessible, instead of only M-A plane as in the case of carbide based MAX. Finite temperature analysis of the mechanical properties further reveals that boron-substitution not only effects the $T = 0$ K mechanical behavior, but also significantly alters the temperature dependence of the mechanical properties. Our exhaustive computational work predicting the modification of a known MAX phase compound with improved mechanical properties, is expected to trigger future experimental activity in terms of synthesis of boron-substituted MAX compounds, and the study of their deformation properties.

II. COMPUTATIONAL DETAILS

The *ab initio* calculations were carried out in plane-wave basis using projector augmented wave (PAW) potentials [21]. The exchange-correlation functional was chosen to be that of generalized gradient approximation (GGA) as implemented in the Perdew-Burke-Ernzerhof (PBE-GGA) formalism [22]. A plane-wave cutoff of 500 eV was found to be sufficient to achieve force convergence of 0.001 eV/Å and total energy convergence of 10^{-8} eV. A slab supercell of dimension $1 \times 1 \times 4$ with 32 atoms, in standard hexagonal crystallographic vectors, $X = [\bar{2}110]$, $Y = [1\bar{2}10]$, $Z = [0001]$ was

created, which was separated by 20 Å of vacuum from its periodic image, to calculate the generalized stacking fault energies (GSFE). A displacement was introduced on a specific basal plane, such that the part of the supercell above this plane glides over the stationary bottom part. The glide planes were chosen to be the ones between V and Al, and V and X atomic layers as shown in Fig. 1. The GSFE was computed as the total energy difference between the unfaulted and faulted systems, defined per unit area of the glide plane. This exercise was carried out systematically for displacements over a fine grid of 18×10 points in the basal planes (0001) at two different cutting levels of V-X ($X = C/B$) and V-Al to obtain the stacking fault energy surfaces, defined as γ surface by Vitek [23]. GSFE along the γ line $[0\bar{1}10]$ was calculated specifically for a quantitative comparison of shearing at two cutting levels and that between boride and carbide.

The continuum model of plastic deformation proposed by Peierls [24] and refined by Nabarro [25] was used to analyze the *ab initio* computed γ surface and to predict characteristics, like Peierls stress and core structure of slip dislocations in different basal planes of the MAX phases.

The model expresses the energy cost associated with a dislocation as a functional of a disregistry function $u(x)$. The total energy cost for dislocation can be split into two parts, i.e., the elastic and misfit energies

$$E[u(x)] = E_{el}[u(x)] + E_{mis}[u(x)], \quad (1)$$

where

$$E_{el}[u(x)] = -K \int_{-\infty}^{\infty} \int_{-\infty}^{\infty} \rho(x)\rho(x') \ln|x-x'| dx dx',$$

and

$$E_{mis}[u(x)] = \int_{-\infty}^{\infty} \gamma[u(x)] dx,$$

$\rho(x) = \frac{du(x)}{dx}$ and $\gamma[u(x)]$ is the γ surface obtained as a function of the basal plane vector. The theoretical concept of Peierls stress σ_p [24], which describes the minimum shear stress required to initiate dislocation at 0 K, was computed by

TABLE I. Elastic constants (C_{ij}), bulk (B), and shear moduli (G) of V_2AlB and V_2AlC . All values are in GPa.

	C_{11}	C_{12}	C_{13}	C_{33}	C_{44}	B	G
V_2AlC	330	74	107	321	149	173	132
V_2AlB	285	86	97	278	120	157	113

considering an additional term [26], $\sigma \int_{-\infty}^{\infty} u_x(x') dx'$ in Eq.(1), and finding the maximum of value of σ (σ_p) exceeding which no stable core solution of the problem can be obtained. For further details see the Appendix.

To compute the temperature dependency of the stacking fault, finite temperature calculations were carried out. The effect of anharmonic phonon was neglected, which was shown to be of negligible contribution up to a temperature of 80% of melting point. Under the assumption that the thermal expansion coefficient of a material remains invariant upon introduction of fault, the effect of finite temperature on faults can be expressed in terms of Helmholtz free energy, by adding ionic vibration to the total energy [27], $F(T) = E_0 + \frac{k_B T}{N_q} \sum_{i,q} \ln[2 \sinh \frac{\hbar \omega_{i,q}}{2k_B T}]$ where, N_q is the number of \mathbf{q} points on a $(48 \times 48 \times 12)$ mesh in the Brillouin zone, and $\omega_{i,q}$ is the frequency of the i th phonon mode at wave vector q .

III. RESULTS

A. Elastic constants

We start our discussion with calculated elastic properties, for the synthesized V_2AlC (VAC) compound, and the proposed boron compound, V_2AlB (VAB). V_2AlB was found to have slightly larger lattice parameters of $a = 2.962 \text{ \AA}$, $c = 13.410 \text{ \AA}$, than that of V_2AlC ($a = 2.927 \text{ \AA}$, $c = 13.252 \text{ \AA}$). The formation enthalpy (ΔH_f), defined as the total energy difference of the MAX phase and the sum of the total energies of the individual elements in their native state, was calculated to be -1.34 and -1.99 eV for V_2AlB and V_2AlC , respectively. This confirms the stability of the boron phase to be formed. The five independent elastic constants for hexagonal lattice of VAB in comparison to VAC, along with their bulk and shear moduli, are listed in Table I. The calculated bulk modulus (B) value of 173 GPa of VAC is consistent with other *ab initio* estimates (175–197 GPa) [17–19] and the value obtained from measurement of sound velocity [20]. We note that B substitution for C reduces the bulk modulus by more than 9% which reflects weakening of the M-X covalent bond. The shear modulus (G) also shows about 14% suppression in B compound compared to C compound. A good measure of machinability [28] is B/C_{44} and that of ductility is B/G [29]. Following this, boride compound is expected to be more machinable as well as more ductile than carbide.

B. Dislocation properties at $T = 0 \text{ K}$

A slip in the basal plane in the layered MAX phase resembles a stacking fault with two partials on either side [23]. Therefore the misfit energy associated with it can be termed as stacking fault energy (SFE), while the stacking fault energy

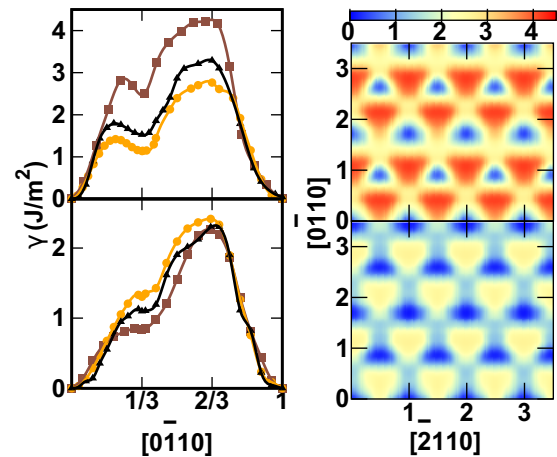


FIG. 2. Left panels: GSFE plots along the $[0\bar{1}10]$ γ line for V-X (top) and V-Al (bottom) cut planes. The brown/squares, orange/circles, and black/triangles represent data for V_2AlC , V_2AlB , and $V_2AlC_{0.5}B_{0.5}$, respectively. Right panels: The γ -surface plots for V-X ($X = B/C$) plane in V_2AlC (top) and V_2AlB (bottom).

associated with all possible translational slips in a particular plane is known as generalized stacking fault energy (GSFE).

During a slip along the $[0\bar{1}10]$ direction, the system encounters a high-symmetry configuration at translation $\mathbf{b}/3$; \mathbf{b} being the Burgers vector in the $[0\bar{1}10]$ direction. In this case, the atoms of the slipping partial rest on symmetric “voids” of the static partial (cf. right panel in Fig. 1). As a result, the GSFE exhibits a local minimum at this configuration, commonly known as the stable stacking fault (SSF) [23]. The energy barrier that precedes the SSFE is named the unstable stacking fault energy (USFE) [30]. Note that the SSF is only observed at $\frac{1}{3}[0\bar{1}10](0001)$ on the γ surface and is therefore of significant importance in determining the quantitative character of the plastic deformation.

The left panels of Fig. 2 show the plot of the calculated γ -line along $[0\bar{1}10]$ for the two cut levels, M-X (upper panel) and M-A (lower panel) for the carbide and boride compounds. We also show the result for the solid solution of two compounds, namely $V_2Al(C_{0.5}B_{0.5})$. The SSF energy (γ_{SSF}) of VAC, which serves as a key parameter in the characterization of plastic deformation [23,30], is found to be much larger in the V-C plane (2.39 J/m^2) compared to that in the V-Al plane (0.91 J/m^2), a feature that is observed in other carbide/nitride MAX phases as well [12]. A remarkable change happens upon substitution of C by B. This reduces the stacking fault energy of the M-X drastically by a factor of 1.5–2. The stacking fault energy of the M-A cut on the other hand, remains more or less unaffected. This, in turn, makes the stacking fault energy of the two cut planes comparable for 100% B-substituted compound, VAB, energies corresponding to SSF of V-B and V-Al planes being 1.1 J/m^2 and 1.3 J/m^2 , respectively.

To characterize the full dislocation core structures in C and B compounds, all significant dislocation characters $[0^\circ$ (Screw), 30° , 60° , 90° (Edge)] defined as the angle between the dislocation line and the Burgers vector need to be computed. This gives rise to the so-called γ -surface plot which

TABLE II. The calculated half-widths of the two partials (ξ_1 and ξ_2), separation of the partials (Δ) and the Peierls stress (σ_p) for the different glide planes in V_2AlC , characterized by different dislocation angles θ . The corresponding values of the calculated parameters for V_2AlB are given in parentheses. The last column lists the percentage decrease in Peierls stress ($\Delta\sigma_p$) for V_2AlB with respect to that of V_2AlC .

θ	ξ_1 (Å)	ξ_2 (Å)	Δ (Å)	σ_p (MPa)	$\Delta\sigma_p$ (%)
V-X (X = B/C) plane					
0(Screw) $^\circ$	0.11(1.5)	0.11(1.5)	1.6(2.1)	1450(718)	50.48
30 $^\circ$	0.10(1.9)	0.11(1.8)	1.5(1.9)	1700(842)	50.47
60 $^\circ$	0.18(1.8)	0.16(1.6)	1.5(2.0)	1550(970)	37.42
90(Edge) $^\circ$	0.14(2.1)	0.14(2.1)	1.6(1.9)	1650(797)	51.69
V-Al plane					
0(Screw) $^\circ$	1.9(1.6)	1.9(1.6)	1.9(2.2)	755(710)	5.96
30 $^\circ$	2.0(1.9)	2.0(2.0)	1.8(1.9)	835(815)	2.39
60 $^\circ$	2.1(2.1)	1.9(2.1)	1.7(2.1)	820(805)	1.82
90(Edge) $^\circ$	2.2(1.8)	2.2(1.8)	2.0(1.7)	840(810)	3.57

contains the information of GSFE in the $[0\bar{1}10]$ - $[\bar{2}110]$ plane. The right panels in Fig. 2 show such plots for the M-X (0001) basal plane, for VAC (upper panel) and VAB (bottom panel). A comparison of the two plots reveals significant suppression of stacking fault energy for M-X layer upon replacement of C by B, as already concluded from γ -line plot along $[0\bar{1}10]$. Additionally, we find a qualitative difference in the dislocation core structure of the two compounds, it being much more diffuse for VAB as opposed to sharp structure in case of VAC. To have a quantitative analysis of this general observation, the dislocation core parameters were obtained with a variational model based on the Peierls-Nabarro formalism. The core structure in this model, as presented in Sec. II, is expressed in terms of disregistry function $u(x)$ where x is in the direction of specific dislocation line. The full width at half-maximum of the derivative of the disregistry function $u(x)$ represent the width of the dislocation core. The plot of $u(x)$ for VAC and VAB as well as derivative of $u(x)$ is shown in the Appendix for the screw direction. We find there is a marked difference in behavior between VAC and VAB. A full dislocation is normally dissociated into two partial dislocations and these partials are separated by stacking fault width (Δ). $du(x)/dx$ is found to be a two peaked structure for VAC, with the spread of the two partials, measured in terms of half-widths (ξ_1 and ξ_2) being nonoverlapping, while $du(x)/dx$ is found to be a single peaked structure for VAB, with the overlapping spread of the two partials. The same trend is observed for other dislocation directions as well, as summarized in Table II. We find that both in case of VAB and VAC the stacking fault width (Δ) is about 2 Å, which is too small for individual partial dislocations to be resolved in transmission electron microscopy (TEM), the typical resolution being few nanometers. The dislocations are thus expected to appear as perfect dislocations, as reported in TEM studies of other MAX compounds [10]. The contrast in the dislocation core structure between VAC and VAB becomes most visible in the computed Peierls stress (σ_p), obtained from Peierls-Nabarro model analysis. Peierls stress quantifies the lattice resistance to dislocation motion and hence is an

TABLE III. Estimate of pairwise bond strengths measured in terms of ICOHP. The bond lengths and γ_{SSF} associated with the corresponding cut plane are also given.

Plane	V_2AlB		V_2AlC	
	V-B	V-Al	V-C	V-Al
ICOHP (eV)	-3.17	-1.68	-3.49	-1.45
Bond length (Å)	2.075	2.739	2.016	2.737
γ_{SSF} (J/m 2)	1.138	1.305	2.391	0.905

important factor dictating the mobility of a dislocation. As is seen from Table II, σ_p for M-A plane for VAB is only 2–6% smaller than that of VAC, while σ_p for M-X plane for VAB shows a large decrease compared to VAC, by about 40–50%. Our $T = 0$ K results thus suggest a qualitative difference in the mechanical behavior of the two compounds at low temperature, with the possibility of activation of two basal slip systems in VAB against a single slip system in VAC. VAB therefore should exhibit larger strain rate than VAC under identical conditions of loading; in other words, should be more ductile.

To understand the difference in the dislocation characteristics between the boride and the carbide MAX phases, one must comprehend the nature of the bonds across the consecutive slip planes. We estimated the bond strength between M-X and M-Al pairs by calculating the crystal orbital Hamiltonian population (COHP). The COHP is defined as the density of states weighted by the corresponding Hamiltonian matrix element. This is a tool that permits energy-resolved analysis of pairwise interactions between atoms. Table III lists the COHPs for M-A and M-X bonds energy integrated until Fermi energy (ICOHP). The stable stacking fault energies are also listed to show a correspondence between ICOHP and γ_{SSF} . As is evident V-B bond is much weaker than the V-C bond, V-B bond-length being larger than V-C bond. This correlates with the fact that the γ_{SSF} in M-X plane of V_2AlB is significantly lower than that in M-X plane of V_2AlC . The weakening of V-B bond in V_2AlB compared to V-C bond in V_2AlC is further evident in the charge density plots presented in left panel of Fig. 3. The computed phonon band structure of the two compounds, presented in right panel of Fig. 3 supports the same. Appreciable softening of phonon modes is observed for VAB as compared to VAC, the effect being most pronounced for the lowest acoustic branches.

C. Dislocation properties at finite temperature

Finally, it is important to study the influence of temperature. We quantify the temperature evolution of stacking fault free energy in terms of the ratio $\Gamma_{SSF}/\Gamma_{USF}$, where Γ_{SSF} and Γ_{USF} are the free energy corresponding to SSF and USF. Figure 4 shows the temperature evolution of $\Gamma_{SSF}/\Gamma_{USF}$ for the M-X and M-A planes for VAC and VAB compounds. Interestingly, we find while this ratio, is more or less temperature independent for the carbide compound, it shows significant temperature dependence for the boride compound. Even more interestingly, we find that the temperature dependence of

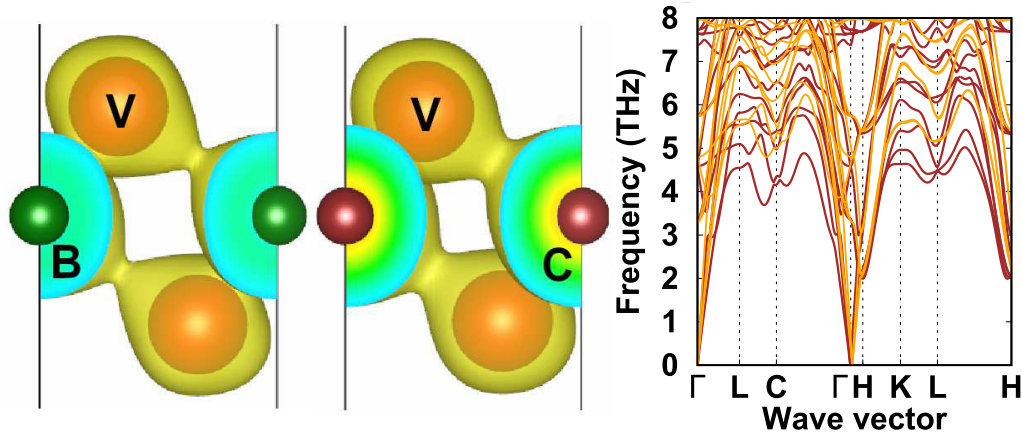


FIG. 3. Left panel: The plot of calculated charge density for V_2A1B and V_2A1C . The isosurface value is chosen at $0.07 e^-/\text{\AA}^3$. Right panel: The phonon band structure of V_2A1B (in brown/dark grey) in comparison to that of V_2A1C (in orange/light grey).

$\Gamma_{SSF}/\Gamma_{USF}$ in VAB to be opposite between the V-A1 and V-B planes. The value of $\Gamma_{SSF}/\Gamma_{USF}$ for V-B plane decreases from a value of 0.8 at 0 K to a value of 0.65 at 1500 K, indicating an increased tendency of formation of wider stacking faults in boride compound at elevated temperature. $\Gamma_{SSF}/\Gamma_{USF}$ for V-A1 plane of VAB, on the other hand, upon increasing temperature, increases from a value slightly below 1 (≈ 0.98) to a value of 1 at a critical temperature of ≈ 730 K, at which USF and SSF configurations become degenerate and the fault vanishes.

IV. CONCLUSION

In the search for a soft MAX phase compound with improved mechanical properties, we studied the mechanical properties of boron-substituted V_2A1C compound. In particular, we computed the generalized stacking fault energies for V_2A1C and B-substituted compounds. The calculated stacking fault energies at $T = 0$ K associated with basal slips between the V-A1 and V-X ($X = B/C$) atomic layers, resulted in the reduction of stable stacking fault energy by a factor of about 1.5–2 in the V-X layer for the boron-substituted compounds, compared to the carbide compound. This makes

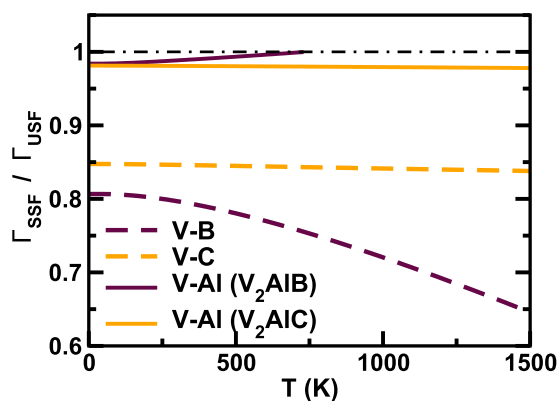


FIG. 4. Temperature evolution of $\Gamma_{SSF}/\Gamma_{USF}$ for two different cut planes and two different compounds.

the SSF of the M-A plane comparable to that of the M-X plane in case of V_2A1B , they being very different in case of V_2A1C . This in turn triggers two basal (M-X and M-A) planes to be operative at $T = 0$ K in case of V_2A1B as opposed to a single basal plane (M-A) in case of V_2A1C . The Peierls stress obtained from the continuum modeling based on inputs of DFT computed γ surface and the elastic constants, shows a significant reduction for M-X layer upon B substitution. Peierls stress being related to mobility of dislocation and being the lower bound of the yield strength, this indicates that the boride MAX phases will be significantly more ductile compared to conventional carbide MAX compounds.

An extension of our study to finite temperature showed that while the stacking faults are not very temperature sensitive for carbide, they show interesting temperature dependence for the boride counterpart, having contrasting temperature dependence of the M-A and M-X slip planes. Curiously, the stable stacking fault in the V-A1 plane of the boron compound becomes more and more unstable as temperature is increased, and finally disappears at ~ 730 K. On the other hand, the SSF for the V-B plane becomes more stable at higher temperature, which implies a well-defined stacking fault to be observed at higher temperatures. The improved mechanical properties of the computer designed boron-based MAX phases, should motivate future synthesis and exploration of these new MAX phases.

ACKNOWLEDGMENTS

This work is supported by the high performance computing facility of Thematic Unit of Excellence on Computational Materials Science at S.N. Bose Centre, funded by Nanomission, Department of Science and Technology, India (Grant No. SR/NM/NS29/2011). P.C. is thankful for useful discussion with Professor M. W. Barsoum.

APPENDIX: DISREGISTRY FUNCTION

The disregistry function $u(x)$ was chosen, following the Volterra model of straight edge dislocation [31]

as

$$u_x(x) = \frac{b}{\pi}[A_1 v_1(x) + A_2 v_2(x)] - \frac{b}{2} \sin \theta,$$

$$u_z(x) = \frac{b}{\pi}[A_3 v_3(x) + A_4 v_4(x)] - \frac{b}{2} \cos \theta,$$

$$v_i(x) = \text{atan}\left(\frac{x - x_i}{c_i}\right); \quad i = 1, 2, 3, 4,$$

$u(x)$ was solved numerically by minimizing $E[u(x)]$ in Eq. (1) with constraints $A_1 + A_2 = \sin \theta$ and $A_3 + A_4 = \cos \theta$, θ being the angle of dislocation.

Figure 5 displays the local dislocation density, $\rho(x) = du(x)/dx$, and the corresponding disregistry function, $u(x)$, for screw dislocations in both V_2A1C and V_2A1B . The effect of replacing carbon by boron is immediately visible in terms of significant increase in widths of the peaks in $\rho(x)$, which correspondingly indicates a wider dislocation core. In the conventional analytical formulations, the Peierls stress varies as $\sim e^{-4\pi\zeta/b}$, where ζ and b are the core width and Burgers vector, respectively. This explains why the Peierls stress in

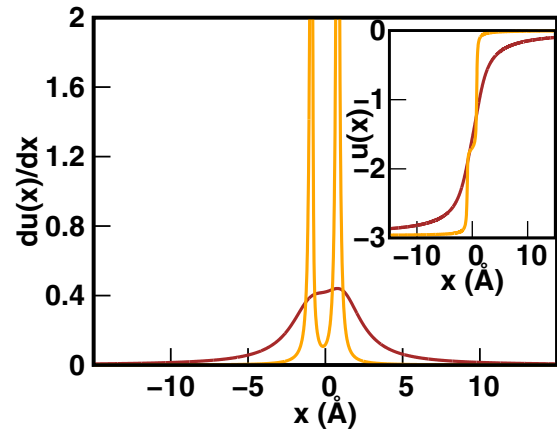


FIG. 5. Plot of the disregistry function $u(x)$ (inset) and its derivative $du(x)/dx$ along the screw direction for V-X (0001) basal plane in V_2A1C (orange/light grey) and V_2A1B (brown/dark grey).

the V-X plane of V_2A1B undergoes a drastic reduction as compared to that in V_2A1C .

- [1] W. Jeitschko, H. Nowotny, and F. Benesovsky, *J. Less Common Metals* **7**, 133 (1964).
- [2] H. Wolfsgruber, H. Nowotny, and F. Benesovsky, *Monatsh. Chem.* **98**, 2401 (1967).
- [3] H. Nowotny, *Prog. Solid State Chem.* **2**, 27 (1970).
- [4] H. Nowotny, J. C. Schuster, and P. Rogl, *J. Solid State Chem.* **44**, 126 (1982).
- [5] M. W. Barsoum and T. El-Raghy, *J. Am. Ceram. Soc.* **79**, 1953 (1996).
- [6] M. W. Barsoum, *Prog. Solid State Chem.* **28**, 201 (2000).
- [7] M. W. Barsoum and T. El-Raghy, *Am. Sci.* **89**, 334 (2001).
- [8] M. W. Barsoum, T. Zhen, S. R. Kalidindi, M. Radovic, and A. Murugaiah, *Nat. Mater.* **2**, 107 (2003).
- [9] M. W. Barsoum and M. Radovic, in *Encyclopedia of Materials Science and Technology*, edited by R. W. Cahn *et al.* (Elsevier, Amsterdam, 2004), pp. 1–11.
- [10] A. Guitton, A. Joulain, L. Thilly, and C. Tromas, *Philos. Mag.* **92**, 4536 (2012).
- [11] A. Guitton, A. Joulain, L. Thilly, and C. Tromas, *Sci. Rep.* **4**, 6358 (2014).
- [12] K. Gouriet, P. Carrez, P. Cordier, A. Guitton, A. Joulain, L. Thilly, and C. Tromas, *Philos. Mag.* **95**, 2539 (2015).
- [13] M. Kabir, S. Mukherjee, and T. Saha-Dasgupta, *Phys. Rev. B* **84**, 205404 (2011).
- [14] P. Chakraborty, T. Das, D. Nafday, L. Boeri, and T. Saha-Dasgupta, *Phys. Rev. B* **95**, 184106 (2017).
- [15] M. W. Barsoum, *Encyclopedia of Materials: Science and Technology* (Elsevier, 2006), pp. 1–11.
- [16] S. Gupta and M. W. Barsoum, *J. Electrochem. Soc.* **151**, D24 (2004).
- [17] J. Wang and Y. Zhou, *Phys. Rev. B* **69**, 214111 (2004).
- [18] Z. Sun, R. Ahuja, S. Li, and J. M. Schneider, *Appl. Phys. Lett.* **83**, 899 (2003).
- [19] Z. Sun, D. Music, R. Ahuja, S. Li, and J. M. Schneider, *Phys. Rev. B* **70**, 092102 (2004).
- [20] S. E. Lofland, J. D. Hettinger, K. Harell, P. Finkel, S. Gupta, M. W. Barsoum, and G. Hug, *Appl. Phys. Lett.* **84**, 508 (2004).
- [21] G. Kresse and J. Hafner, *Phys. Rev. B* **47**, 558 (1993).
- [22] J. P. Perdew, K. Burke, and M. Ernzerhof, *Phys. Rev. Lett.* **77**, 3865 (1996).
- [23] V. Vitek, *Crystal Latt. Def.* **5**, 1 (1974).
- [24] R. E. Peierls, *Proc. Phys. Soc.* **52**, 34 (1940).
- [25] F. R. N. Nabarro, *Proc. Phys. Soc.* **59**, 256 (1947).
- [26] V. Bulatov and W. Cai, *Computer Simulations of Dislocations*, edited by A. P. Sutton (Oxford University Press, New York, 2006).
- [27] A. van de Walle and G. Ceder, *Rev. Mod. Phys.* **74**, 11 (2002).
- [28] Z. Sun, D. Music, R. Ahuja, and J. M. Schneider, *Phys. Rev. B* **71**, 193402 (2005).
- [29] S. F. Pugh, *Philos. Mag.* **45**, 823 (1954).
- [30] S. Aubry and D. A. Hughes, *Phys. Rev. B* **73**, 224116 (2006).
- [31] V. Volterra, *Ann. Scient. Ec. Norm. Sup.* **24**, 401 (1907).